C Journal of Carbon Research

MDPI

Article

Improving the Wear and Corrosion Resistance of Titanium Alloy Parts via the Deposition of DLC Coatings

Alexander Metel [1], Catherine Sotova [1], Sergey Fyodorov [1], Valery Zhylinski [2], Vadzim Chayeuski [3], Filipp Milovich [4], Anton Seleznev [1], Yuri Bublikov [5], Kirill Makarevich [1] and Alexey Vereschaka [5,*]

[1] Department of High-Efficiency Machining Technologies, Moscow State University of Technology "STANKIN", Vadkovsky Lane 3a, 127055 Moscow, Russia; a.metel@stankin.ru (A.M.); e.sotova@stankin.ru (C.S.); sv.fedorov@stankin.ru (S.F.); a.seleznev@stankin.ru (A.S.); mkm@c-plus.pro (K.M.)
[2] Department of Chemistry, Technology of Electrochemical Production and Electronic Materials, Belarusian State Technological University, 13a, Sverdlov Street, 220006 Minsk, Belarus; zhilinski@yandex.ru
[3] Department of Physics, Faculty of Information Technology, Belarusian State Technological University, 13a, Sverdlov Street, 220006 Minsk, Belarus; doctorv_v_ch@mail.ru
[4] Materials Science and Metallurgy Shared Use Research and Development Center, National University of Science and Technology "MISiS", Leninsky Prospect 4, 119049 Moscow, Russia; filippmilovich@mail.ru
[5] Institute of Design and Technological Informatics of the Russian Academy of Sciences (IDTI RAS), Vadkovsky Lane 18a, 127055 Moscow, Russia; yubu@rambler.ru
* Correspondence: dr.a.veres@yandex.ru; Tel.: +7-9169100413

Abstract: This article compares the properties of the diamond-like carbon (DLC) coating with those of ZrN and (Zr,Hf)N coatings deposited on the Ti-6Al-4V titanium alloy substrate. To improve substrate adhesion during the deposition of the DLC coating, preliminary etching with chromium ions was conducted, ensuring the formation of a chromium-saturated diffusion surface layer in the substrate. A Si-DLC layer followed by a pure DLC layer was then deposited. The hardness of the coatings, their surface morphology, fracture strength in the scratch test, and tribological properties and wear resistance in the pin-on-disk test in contact with Al_2O_3 and steel indenters were investigated. The structure of the DLC coating was studied using transmission electron microscopy, and its corrosion resistance in an environment simulating blood plasma was also investigated. In the pin-on-disk test in contact with Al_2O_3 and AISI 52100 indenters, the DLC-coated sample demonstrates a much lower friction coefficient and significantly better wear resistance compared to the nitride-coated and uncoated samples. Both nitride coatings—(Zr,Hf)N and ZrN—and the DLC coating slow down the corrosive dissolution of the base compared to the uncoated sample. The corrosion currents of the (Zr,Hf)N-coated samples are 37.01 nA/cm^2, 20% higher than those of the ZrN-coated samples. The application of (Zr,Hf)N, ZrN, and DLC coatings on the Ti-6Al-4V alloy significantly inhibits dissolution currents (by 30–40%) and increases polarization resistance 1.5–2.0-fold compared to the uncoated alloy in 0.9% NaCl at 40 °C. Thus, the DLC coating of the described structure simultaneously provides effective wear and corrosion resistance in an environment simulating blood plasma. This coating can be considered in the manufacture of medical products (in particular, implants) from titanium alloys, including those functioning in the human body and subject to mechanical wear (e.g., knee joint endoprostheses).

Keywords: diamond-like carbon; wear resistance; corrosion resistance; titanium alloy; coating

Citation: Metel, A.; Sotova, C.; Fyodorov, S.; Zhylinski, V.; Chayeuski, V.; Milovich, F.; Seleznev, A.; Bublikov, Y.; Makarevich, K.; Vereschaka, A. Improving the Wear and Corrosion Resistance of Titanium Alloy Parts via the Deposition of DLC Coatings. *C* **2024**, *10*, 106. https://doi.org/10.3390/c10040106

Academic Editors: Jinliang Song and Craig E. Banks

Received: 27 September 2024
Revised: 5 December 2024
Accepted: 12 December 2024
Published: 16 December 2024

1. Introduction

Diamond-like carbon (DLC) coatings have found wide application in various fields of modern industry due to a number of useful properties. In addition to their high hardness and wear resistance, they are distinguished by high chemical passivity and corrosion resistance [1–6]. Although relatively low heat resistance and the tendency for diffusion and dissolution in iron limit the application of DLC in the production of cutting tools,

these coatings are effective as anti-corrosion and wear-resistant materials at operating temperatures below 450 °C, which is acceptable for most applications. The disadvantages of DLC coatings include high internal stresses; these can lead to poor substrate adhesion [5–10] and result from energetic ion bombardment during deposition [11]. Furthermore, studies have noted that the internal stresses in DLC coatings can arise from both the inherent stress generated during coating deposition and the thermal stress induced by the mismatch in the coefficient of thermal expansion between the DLC coating and the substrate materials [12]. In addition to causing poor substrate adhesion of the coating, these stresses promote the formation of microcracks, together leading to premature coating failure. Adhesion can be improved through the deposition of transition (adhesion) layers (usually Cr-CrN, W, or Si with various additives) and pretreatment of the deposition surface (particularly via plasma nitriding or laser microprofiling) [2,3,13]. The introduction of Cr-CrN intermediate layers ensures strong adhesion of the DLC coating to the substrate [14]. However, researchers have also reported the insufficient adhesion strength of DLC coatings with an intermediate Cr or Cr-CrN layer, leading to the rapid destruction of the coatings [15–17]. Compared with single-layer DLC coatings, multilayer DLC coatings with Cr-CrN or Cr-W-DLC transition structures exhibit improved strength, while the content of sp^3 covalent bonds is reduced. This indicates a significant improvement in the adhesion strength and impact toughness of the multilayer coatings and a significant reduction in the residual stress [18,19].

While high internal stresses impair substrate adhesion, the main contribution to the high wear resistance of the DLC coating arises from compressive stresses formed during its deposition, both in the coating itself and in the outer layers of the substrate [20,21].

The corrosion resistance of DLC-coated samples has been investigated in various environments. For example, the anticorrosive properties of the Cr-CrN-DLC coating deposited on the Ti-6Al-4V alloy substrate have been studied with regard to electrochemical corrosion in a 3.5% NaCl solution [1]; after testing, the oxygen content on the Cr-CrN-DLC surface was lower than that on the surface of the uncoated and nitrided titanium alloys. The sample with the Cr-CrN-DLC coating also had the lowest corrosion current density, i_{corr}, and the highest polarization resistance, Rp. In another study, the Cr-CrN-DLC coating deposited on a St37 steel substrate reduced the corrosion current density in a 3.5 wt% NaCl solution from 1.19 to 0.53 $\mu A/cm^2$ and increased the polarization resistance from 33.93 to 76.66 kΩ [22]. Furthermore, the properties of DLC coatings with various combinations and structures of intermediate layers (nitrided, organosilicon, and gas flow gradient layers) have been explored [23]. The optimal wear resistance in combination with corrosion resistance in a 3.5% NaCl solution was provided by the coating with the full set of specified intermediate layers; however, the exclusion of the organosilicon layer only slightly reduces the coating properties. Researchers have also compared the anticorrosive properties of DLC and W-DLC coatings deposited on CF170 steel samples in the presence and absence of preliminary plasma nitriding [24]. According to the potentiodynamic polarization curves during the study in 0.5 mol/L H_2SO_4 solution, the DLC-coated sample subjected to preliminary plasma nitriding showed the lowest corrosion current density and the highest corrosion potential. Another study investigated the corrosion resistance of DLC-, Cr/DLC-, H/DLC-, and WC/DLC-coated samples in a hydrochloric acid (HCl) environment [25], with the DLC coating exhibiting the lowest wear rate in 1 M HCl. Since silver (Ag) is a powerful antibacterial agent, Ag–DLC coatings have been suggested as potentially useful in biomedical applications [26].

DLC coatings are not the only choice for providing high wear and corrosion resistance; a notable alternative involves coatings based on the nitrides and carbonitrides of various metals. Thus, implants composed of the titanium alloy Ti-6Al-4V with a TiN coating have shown good biocompatibility and bone-bonding properties [27]. In another study, the corrosion resistance of SST 304 steel samples with (Cr,Al,Ti)N and CrN/NbN coatings was investigated in a $CaCl_2$ environment [28]. The sample with the CrN/NbN coating displayed the best corrosion resistance, while both coatings offered good biocompatibility. Research has also shown that the deposition of a ZrN coating on a Ti-6Al-4V sample pro-

vides good corrosion resistance when exposed to saline and reduces the bioadhesion of *Staphylococcus aureus* bacteria [29]. Moreover, in [30], concerning the bioadhesion of *Staphylococcus aureus* on Ti–TiN, Zr–ZrN, Zr–(Zr,Nb)N, and Zr–(Zr,Hf)N coatings, the maximal density of bacterial colonization was observed on the TiN and (Zr,Hf)N surfaces over a 30-day period at 25 °C. Another study compared the corrosion resistance of TiN, ZrN, CrN/TiN, and CrN/ZrN coatings deposited on a Ti-6Al-4V substrate [31]; the CrN/ZrN-coated sample showed the optimal corrosion resistance, and the ZrN and CrN/ZrN coatings provided the best biocompatibility and better hydroxyapatite deposition. Furthermore, the inclusion of hafnium in the ZrCN coating increases the corrosion resistance in Ringer's solution and biocompatibility [32]. According to [29–32], biocompatibility depends on several factors, including corrosion resistance, surface microroughness, etc. High corrosion resistance prevents metal ions from penetrating living tissue, eliminating the possibility of poisoning living cells and increasing biocompatibility. On the other hand, the corrosion process generates microroughness, which promotes the bioadhesion of living cells. The latter may be a decisive factor in the colonization of the coating surface by *Staphylococcus aureus* colonies [29–32]. In another study, the (Ti,Zr)N coating provided better wear and corrosion resistance in Hank's solution compared to uncoated and TiN-coated titanium alloy samples [33]. A study of the tribocorrosion effect on Zr/ZrN-coated samples in a simulated body fluid (SBF) showed that the multilayer Zr/ZrN coating exhibits better corrosion resistance than the single-layer ZrN coating [34]. The (Zr,Hf)N coating is very hard and, at the same time, quite brittle [35]; its oxidation leads to the formation of ZrO_2 and HfO_2 phases, decreasing its hardness [36]. At high temperatures, the formation of a double oxide, $(Zr,Hf)O_2$, has been observed in the (Zr,Hf)N coating [37,38]. Furthermore, the introduction of hafnium into the ZrN system provides increased oxidation resistance [39]. The effect of hafnium on oxidation resistance in the corrosion process in the (Zr,Hf)N coating is considered in [40]; electrochemical investigations established that the introduction of hafnium leads to an increase in the polarization resistance of the coating due to the formation of a dense nonconductive layer of Zr,Hf oxonitride. The resulting layer protects the (Zr,Hf)N coatings from further oxidation [40].

The properties of DLC coatings and nitride coatings of various compositions have been compared. Two-component TiN or CrN coatings deposited on a Ti-6Al-4V titanium alloy substrate have shown greater wear resistance compared to TiN/CN and TiC/C coatings. However, they are inferior to DLC coatings of various structures—hydrogen-free tetrahedral carbon coatings (ta-C); amorphous carbon (a-C) or graphite-like coatings; and hydrogenated amorphous carbon (a-C:H) [4]. The authors attribute the favorable properties of the a-C:H coating to its good substrate adhesion. Its hardness is slightly lower than that of the counterbody material but is still rather high, its elastic modulus is similar to that of the counterbody material, and it can form soft surface films on both counterbodies. The anticorrosive properties of ZrN and ta-C (tetrahedral amorphous carbon) coatings have also been compared [41], with the ZrN-coated sample displaying better adhesion between the coating and substrate, improved corrosion resistance, microhardness, and wettability. A comparative study of the effect of titanium implants with TiN, ZrN, and DLC a-C:H coatings on the animal body did not reveal significant differences between the tested materials [42]. In all three cases, no implant-related inflammatory reaction or foci of necrosis were detected.

Electrochemical salt spray tests and immersion tests have been carried out to study the effect of aggressive environments (NaCl, H_2SO_4, HCl, and NaOH) on the corrosion properties of multilayer silicon-doped DLC coatings. According to the impedance study, the interfacial contact resistance (Rc) of the DLC coating is $9.4 \times 10^7\ \Omega \times cm^2$ in 3.5 wt% NaCl solution [43]. In [44], researchers found that the DLC coating on 316L stainless steel, CoCrMo, and Ti-6Al-4V substrates exhibited similar structures. The failure mechanism of the DLC coatings on 316L stainless steel and the CoCrMo alloy during friction tests (where Al_2O_3 balls were used as friction pairs) involved coating delamination, while the DLC coating on Ti-6Al-4V showed good wear resistance and stability due to its favorable

adhesion and anticorrosion properties. The DLC coating exhibits enhanced adhesion on the titanium alloy substrate compared to the stainless steel one because the chemical bond energy holding Ti atoms (titanium alloy surface) and C atoms together is the strongest [44].

The corrosion behavior of DLC-coated SUS316L steel was studied via the potentiostatic polarization of coated samples in a 0.5 M H_2SO_4 solution at +0.8 V and 90 °C for 168 h [45]. From the analysis of the SUS316L steel and DLC-coated SUS316L polarization curves, the corrosion potential of the latter reached approximately +0.1 V, significantly higher than that of the former (approximately −0.2 V). The increase in the corrosion potential of the coating during the corrosion process is associated with the formation of oxygen-containing groups on the surface of the DLC and the process of metal passivation. Under fuel cell operating conditions, the corrosion current density was approximately 19 μA/cm^2 for SUS316L steel and at least 0.5 μA/cm^2 for DLC-coated steel. The reduction in the corrosion current density for DLC-coated SUS316L steel is due to the protective effect of the DLC itself, which shields the steel from direct interaction with H_2SO_4.

Thus, both ZrN-based nitride coatings and the DLC coating provide high wear and corrosion resistance, which allows them to improve the resistance of titanium alloy parts. This work aims to compare the properties of these coatings to determine the optimal choice for use in aggressive environments combined with mechanical wear.

A possible area of application for titanium parts with the considered coatings is medical implants with friction pair elements operating in the human body (e.g., knee joint endoprostheses). While medical implants form the key application area of the developed coatings, other areas of application in which titanium products are required to simultaneously exhibit good wear and corrosion resistance are also possible (e.g., shut-off valves of nuclear power plant pipelines and other shut-off valves of critical units). Based on real operating conditions, titanium parts can be in contact with both hard ceramic parts (which are well imitated by Al_2O_3) and softer, more ductile counterbodies (well imitated by AISI 52100). Thus, contact in a tribo-pair with two substantially different counterbodies was considered. DLC coatings are widely used to modify the surface of titanium alloy products. Nitride coatings could offer a good alternative to DLC coatings due to their improved crack resistance and resistance to brittle fractures, with high resistance to mechanical wear and corrosion. In this paper, the goal was to compare the DLC coating with the two nitride coatings—(Zr,Hf)N and ZrN—which have shown better results in terms of both mechanical wear and corrosion resistance in previous studies [40,46].

2. Materials and Methods

2.1. Deposition of DLC Coatings

The plasma-enhanced chemical vapor deposition of carbon condensates was used to deposit the DLC coating on a Platit setup (π311 + DLC, Platit, Selzach, Switzerland) by decomposing the components of the gas mixture [47]. At the start of the process, the samples were cleaned in a gas discharge and etched with chromium ions at a reference voltage of −750 V on the products, after which the process temperature was reduced to 200 °C. Tetramethylsilane, $(CH_3)_4Si$ (TMS), was fed into the vacuum chamber, bringing its content in the gas mixture to 80% to ensure adhesion between the layers. A voltage of −500 V was applied to the products, and a glow discharge was ignited. DLC was grown for 1 h and 40 min at a gas mixture ratio of 95% C_2H_2, 4% Ar, and 1% TMS at a pressure of 0.8 Pa.

2.2. Deposition of Nitride Coatings

The deposition of nitride coatings was carried out on the VIT-2 installation (IDTI RAS—MSUT "STANKIN", Moscow, Russia) [37,48], and Controlled Accelerated Arc (CAA-PVD) technology was used during the deposition [49,50]. Zr (99.98%) cathodes and a Zr-Hf (50:50, %) alloy cathode were used. During the coating deposition, the arc current of the zirconium cathodes was 80 A, and that of the Zr-Hf (50:50, %) cathode was 90 A. The remaining parameters were the same for all processes: nitrogen pressure, 0.42 Pa; substrate voltage,

−150 V; and tool rotation speed, 0.7 rpm. The difference in the arc currents of the Zr and Zr-Hf cathodes is explained by the significantly higher melting point and mass of hafnium. Accordingly, a higher current is required to form a stable arc.

2.3. Preparation of Samples Before Coating Deposition

Before the deposition of the coatings, the samples were prepared using a universal method for nitride and DLC coatings:

- washing with a neutral detergent at 80 °C with ultrasonic stimulation;
- rinsing in purified running water;
- drying in a stream of hot filtered air.

2.4. Mechanical Properties of Coated Samples

The scratch test was carried out using a CB-500 tester (Nanovea, Irvine, CA, USA) in accordance with the ASTM C1624-22 method [51]. A diamond indenter with a tip radius of 100 μm was used.

The wear resistance was studied according to the ASTM "Standard Test Method for Wear and Friction Testing with a Pin-on-Disk or Ball-on-Disk Apparatus" [52]. A 6 mm-diameter spherical indenter composed of Al_2O_3 and AISI 52100 steel, at a load of 10 N and a rotation speed of 100 rpm, was used, and the test duration was 1 h. The test was conducted at room temperature without any lubricant. The wear results are presented as the volume loss in cubic millimeters for the test sample (coated disk) and as the mass loss for the ball.

The hardness and elastic modulus were investigated on a nanotester SV-500 (Nanovea, Irvine, CA, USA) using a Berkovich indenter, at a maximum load of 20 mN. The average values were determined based on 20 measurements.

The surface morphology and structure of the coatings were studied using a Carl Zeiss (Oberkochen, Baden-Württemberg, Germany) EVO 50 scanning electron microscope (SEM), with an EDX system X-Max—80 mm^2 (OXFORD Instruments, Abingdon, Oxfordshire, UK), and a transmission electron microscope (TEM), TEM JEM 2100 (JEOL, Tokyo, Japan). The elemental composition was studied using a TEM with EDX INCA Energy (OXFORD Instruments, Abingdon, Oxfordshire, UK). TEM samples were prepared using a focused ion beam (FIB) on a Strata 205 device (FEI Company, Hillsboro, OR, USA).

2.5. Corrosion Studies

Electrochemical corrosion studies of the coatings on the Ti-6Al-4V titanium alloy were carried out via cyclic voltammetry (potential scan rate = 1 mV/s) with an electrode polarization of ±800 mV using the potentiostat-galvanostat AUTOLAB PGSTAT302 N (Utrecht, The Netherlands). The experiments were performed in a physiological solution (0.9 wt% NaCl) in a standard three-electrode electrochemical cell (YSE-2) with a graphite auxiliary electrode and a saturated silver chloride reference electrode at 40 °C. The area of the working electrode was 1 cm^2. All potential values measured relative to the reference electrode were converted to the scale of the standard hydrogen electrode. The corrosion currents were calculated via mathematical modeling functions of the corrosion process in the Nova 2.0 program and using the polarization resistance method based on experimental data at low polarizations (η = ±20 mV), as given in Equation (1):

$$\eta \approx \frac{RT}{nF}\frac{i}{i_0} = R_0 i, \quad (1)$$

where $R_0 = \frac{RT}{i_0 nF}$ is the charge transfer resistance, Ω [46].

3. Results

3.1. Surface Morphology, Hardness, and Scratch Resistance

A moderate amount of microparticles can be observed on the surface of the ZrN and (Zr,Hf)N coatings, without significant structural defects (Figure 1). Furthermore, on the surface of the (Zr,Hf)N coating, there are local structural defects associated with the effect of microparticles on the coating (Figure 1d–f). The presence of such microparticles can be associated with the effect of the presence of hafnium [40], which is significantly heavier (atomic mass = 178.49) and refractory (melting point = 2233 °C) compared to zirconium (atomic mass = 91.22; melting point = 1852 °C) [53].

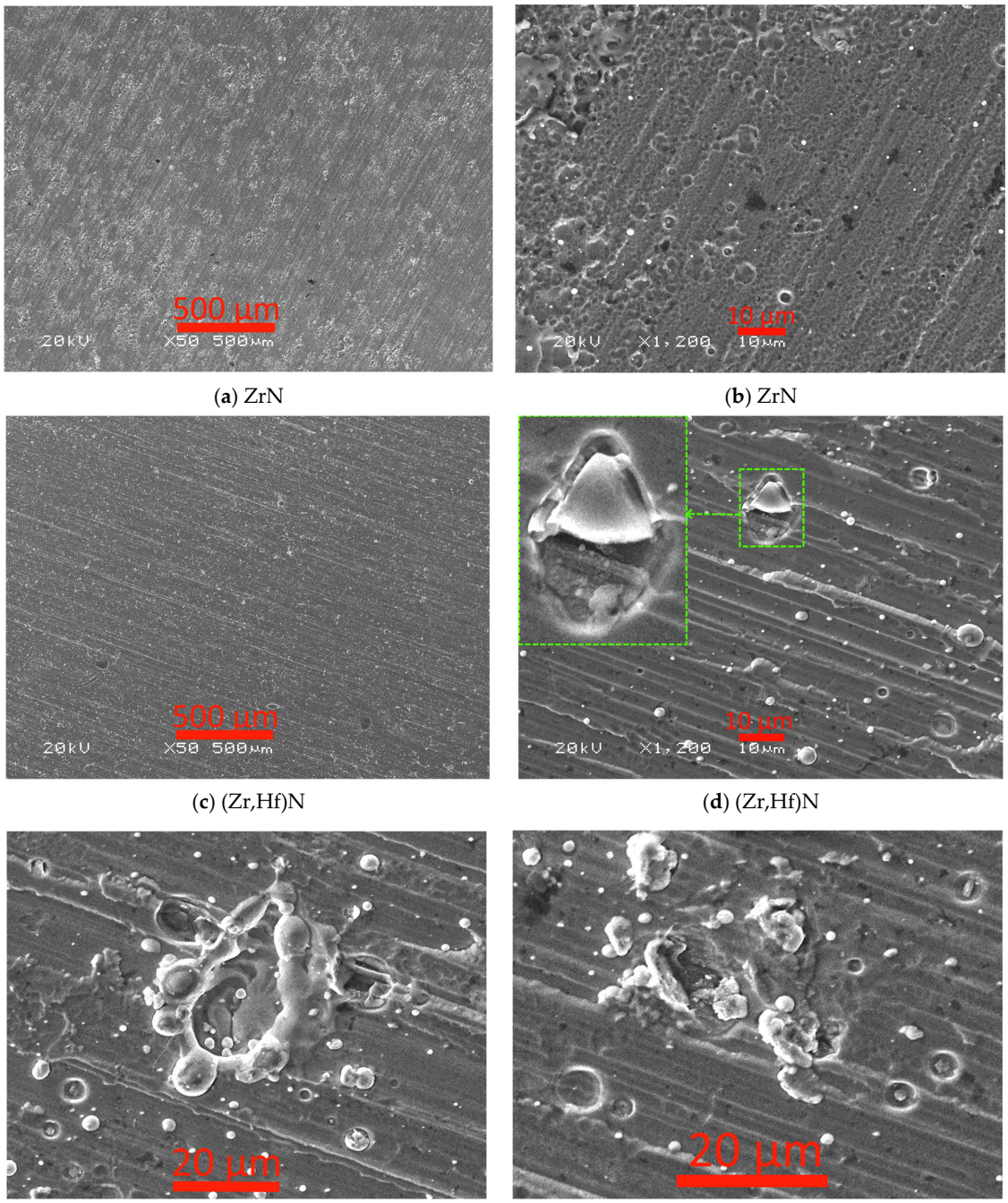

(**a**) ZrN (**b**) ZrN

(**c**) (Zr,Hf)N (**d**) (Zr,Hf)N

(**e**) (Zr,Hf)N (**f**) (Zr,Hf)N

Figure 1. Surface morphology of (**a**,**b**) ZrN and (**c**) (Zr,Hf)N coatings; and (**d**–**f**) structural defects of the (Zr,Hf)N coating (SEM).

A significant number of spherical microparticles can be observed on the surface of the DLC coating (Figure 2a,b). A characteristic surface defect of this coating is potholes up to 100 µm in size (Figure 2c–f), the formation of which may be due to a high level of internal stresses in combination with the high brittleness of the coating [5,6].

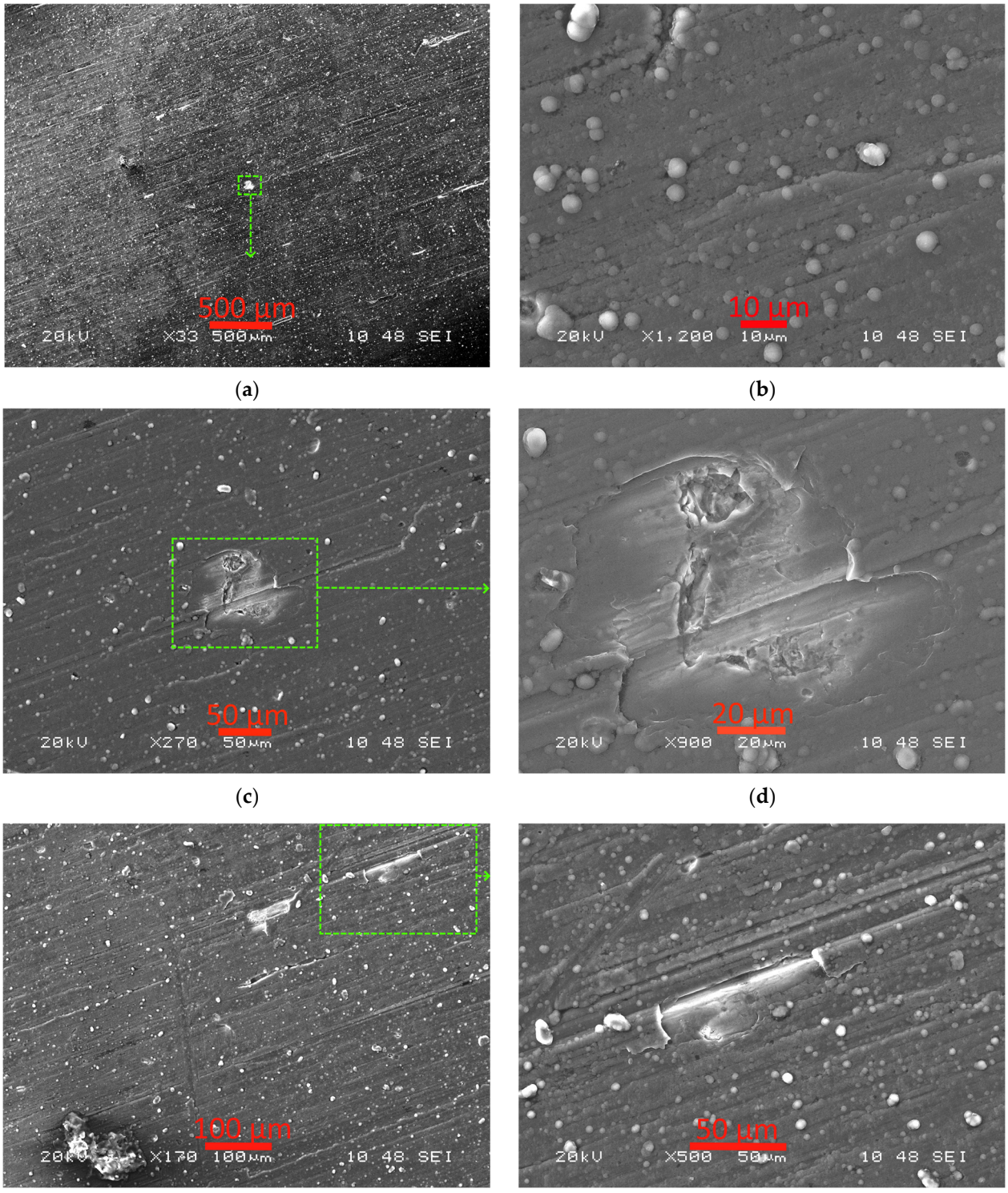

Figure 2. (**a**,**b**) Surface morphology of DLC coatings and (**c**–**f**) structural defects of the coating (SEM).

The structure of the DLC coating involves a diffusion layer on the surface of the titanium substrate (saturated with chromium due to ion etching with metallic chromium ions, see Figure 3), a DLC + Si layer approximately 200 nm thick, and a base DLC layer approximately 4 μm thick.

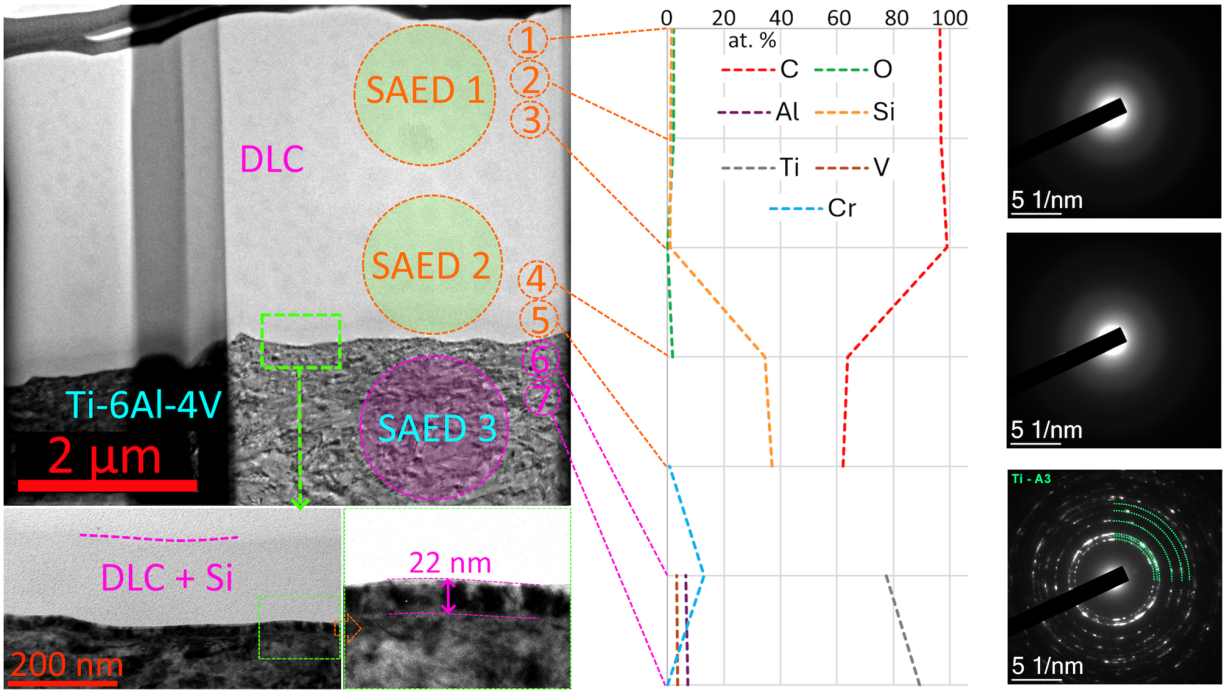

Figure 3. Internal structure (TEM) and elemental and phase (SAED) composition of DLC coating.

Selected area diffraction (SAED) studies reveal the presence of the Ti (A3) phase in the substrate and the amorphous structure of the DLC coating. The ZrN and (Zr,Hf)N coatings also have a thickness of approximately 4 μm.

A comparison of the coating hardness reveals that the ZrN coating has the minimum (29.35 ± 1.42 GPa) while DLC has the maximum (45.17 ± 0.63 Gpa) hardness among the studied coatings. The hardness of the (Zr,Hf)N coating is 32.85 ± 1.18 Gpa. The hardness of the DLC coating is characterized by a significantly smaller spread of values, which may be due to the greater homogeneity of its structure.

The results of scratch tests reveal the relatively high strength of the ZrN coating failure—the coating failure (point LC_2) begins at a load of approximately 21 N, and the first signs of the onset of failure (point LC_1) correspond to a load of approximately 16 N (Figure 4a). The nature of the failure of the ZrN coating can be attributed to the compressive tension failure type [54].

The (Zr,Hf)N coating Is also characterized by a fairly high fracture strength—the coating fracture (point LC_2) begins at a load of approximately 18 N, and the first signs of the onset of fracture (point LC_1) correspond to a load of roughly 7 N (Figure 4b). The fracture pattern of this coating is most consistent with bending-induced conformal cracking [54].

The failure of the DLC coating Is rather difficult to Identify using the acoustic emission signal since a high level of this signal is observed immediately after the start of the tests, remaining virtually unchanged throughout the tests (Figure 4c). Based on the visual observations, one can conclude that for this coating, fracture (point LC_2) begins at a load of approximately 16 N, and the first signs of the onset of fracture (point LC_1, determined based on the analysis of the groove image) correspond to a load of roughly 6 N. The fracture pattern of the DLC coating can be described as spallation failure [54]. From the scratch test perspective, DLC coatings exhibit the greatest problems with substrate adhesion, as noted earlier [5–10].

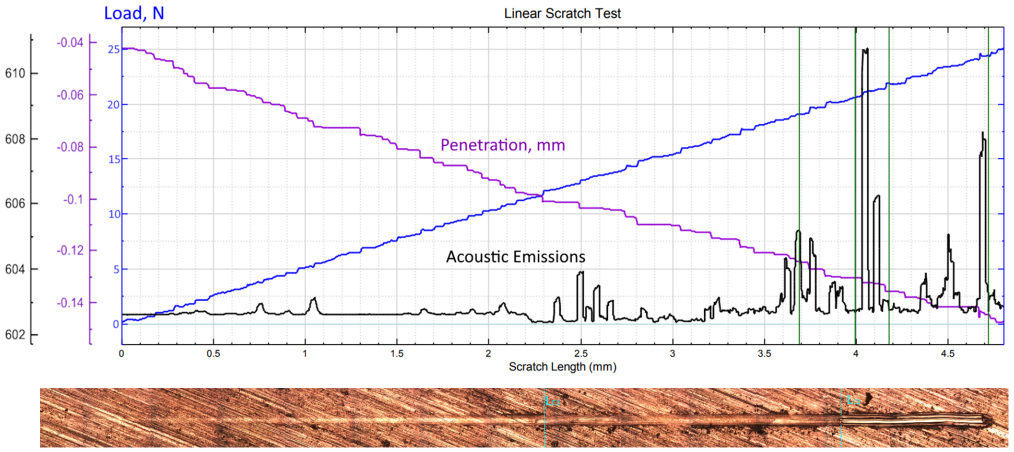

(**a**) ZrN

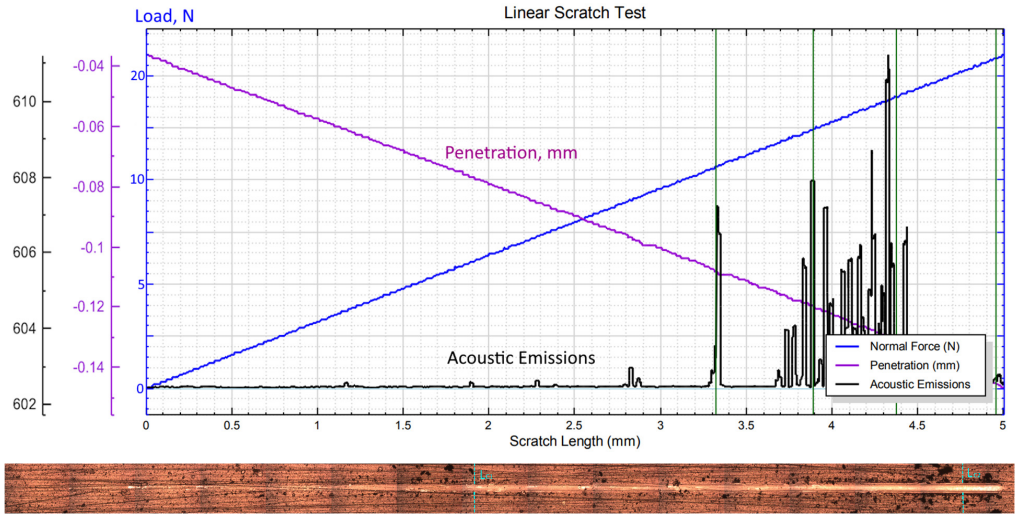

(**b**) (Zr,Hf)N

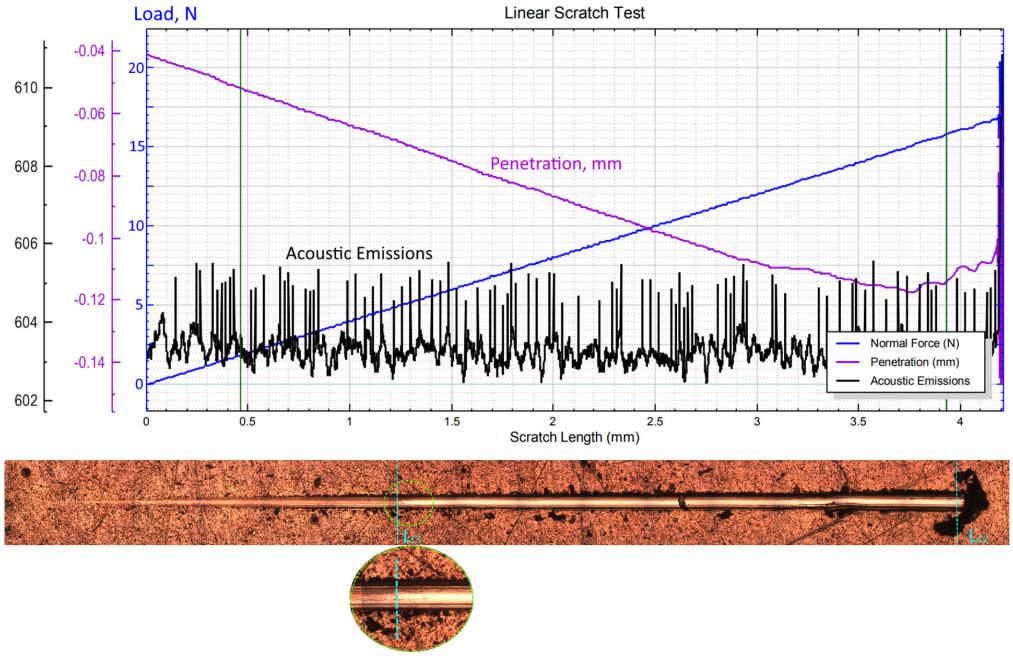

(**c**) DLC

Figure 4. Acoustic emission data (**top**) and general view of the scribing groove (**bottom**) for the (**a**) ZrN, (**b**) (Zr,Hf)N, and (**c**) DLC coatings.

As depicted in Figure 5, the DLC coating failure at the scribing groove boundary involves the active formation of cracks cutting through the coating structure (Figure 5a). The dominant mechanism of the coating failure is brittle failure with the formation of chips.

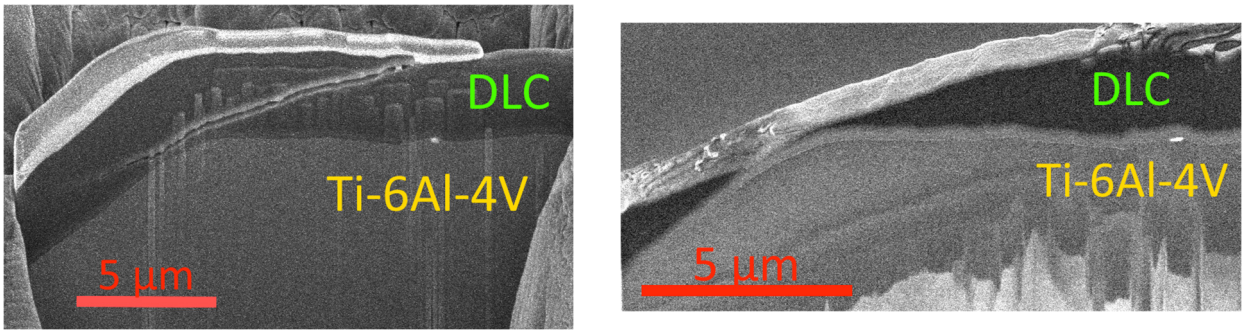

(**a**) (**b**)

Figure 5. The surface structure and nature of DLC coating destruction during scratch test: (**a**) formation of a crack in the coating structure, and (**b**) the nature of coating destruction at the boundary of the scribing groove (SEM).

3.2. Tribological Properties and Wear Resistance

Since titanium alloy parts are widely used in various fields of human activity, it is possible to operate such parts in tribological contact with counterbodies of different compositions. In this study, we considered both ceramic (Al_2O_3) counterbodies (indenters), with a significantly higher hardness compared to titanium, and counterbodies composed of AISI 52100 steel, with hardness values quite close to titanium. Several studies of DLC-coated samples have been conducted using the pin-on-disk method [11]. However, since their experimental conditions differ significantly, it is impossible to compare the obtained results. Therefore, comparisons of different coatings carried out under identical conditions are of great importance. The appearance of wear tracks of the samples after pin-on-disk testing is shown in Figure 6.

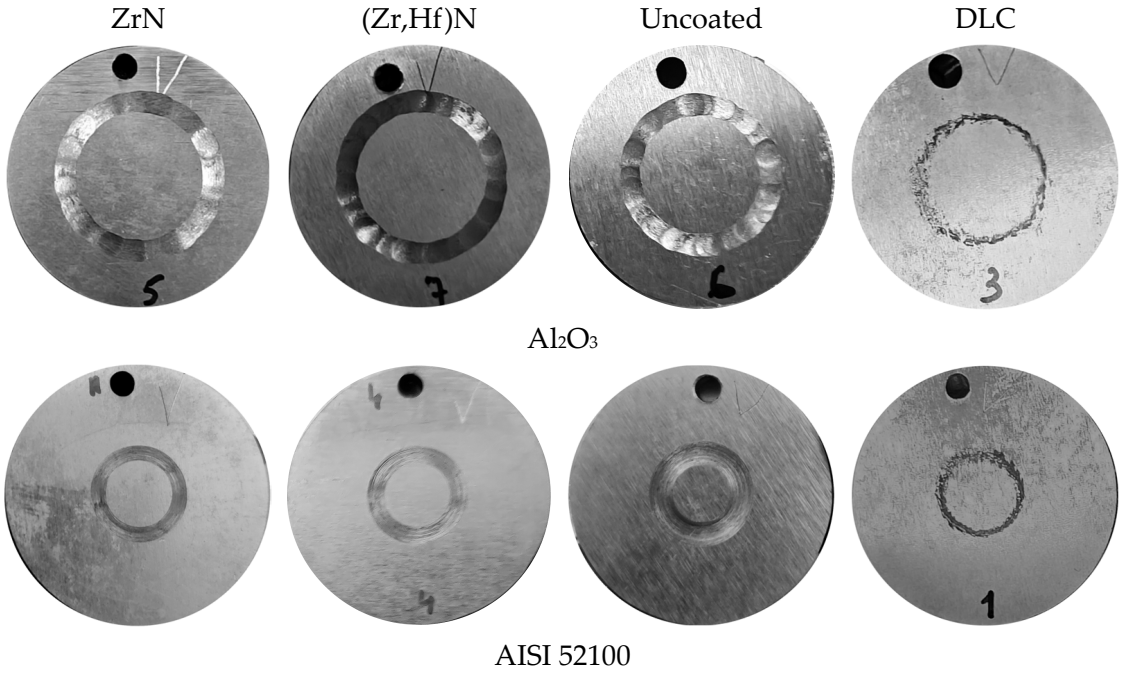

Figure 6. Appearance of wear tracks of samples after pin-on-disk testing.

Figure 7a,b compare the tribological properties of the coated and uncoated samples in contact with the Al_2O_3 and AISI 52100 indenters. The DLC-coated sample shows the lowest coefficient of friction (COF) for both indenters. The low COF value for the DLC-coated sample compared to the nitride coatings has been noted in previous studies [55]. At the same time, the ZrN- and (Zr,Hf)N-coated samples display a noticeable decrease in the COF in contact with the Al_2O_3 indenter. However, when in contact with the AISI 52100 indenter, only the (Zr,Hf)N coating exhibits a decrease in the COF, while the ZrN-coated sample yields identical results to the uncoated sample. It is worth noting that when in contact with the AISI 52100 indenter, the ZrN-coated sample yields a lower COF value compared to the (Zr,Hf)N coating. A previously conducted comparison of the tribological properties of ZrN- and DLC-coated samples when in contact with various counterbodies (with different hardness values, from steel to diamond) revealed that in all cases, the ZrN-coated samples showed a significantly higher COF value [56]. Moreover, as the hardness of the counterbodies increased, the difference in the COF value initially increased and then decreased. In our case, a similar effect was observed—for the significantly harder Al_2O_3 indenter, the difference in the COF values between the ZrN- and DLC-coated samples is less than in the tribological pair with an indenter made of the softer AISI 52100 steel.

Figure 7c,d compare the wear resistance of the coated and uncoated samples. Notably, the DLC-coated sample provides significantly better wear resistance compared to the other samples in all cases. When in contact with the Al_2O_3 indenter, wear of the DLC-coated sample is not observed, possibly due to the hardness of Al_2O_3 (16–20 GPa [57,58]) being significantly closer to that of DLC compared to AISI 52100 (8 Gpa [59]). Thus, a very low friction coefficient arises between the bodies in the friction pair since their adhesive Interaction Is minimal. Accordingly, under these experimental conditions, the wear of the DLC-coated sample is not recorded, but there is an insignificant loss of mass by the Al_2O_3 indenter (Figure 7e). When the DLC-coated sample and the AISI 52100 indenter come into contact, insignificant wear of the sample is observed; this can be associated with both adhesive interactions and the dissolution of carbon from the DLC in the Indenter Iron.

The wear resistance of the ZrN- and (Zr,Hf)N-coated samples is higher than that of the uncoated sample in all cases but lower than that of the DLC-coated sample. Furthermore, when in contact with the Al_2O_3 indenter, the (Zr,Hf)N-coated sample shows the optimal wear resistance, while in the case of contact with the AISI 52100 indenter, the best wear resistance arises from the ZrN-coated sample. Previously conducted wear resistance tests of (Zr,Hf)N-coated samples using Al_2O_3 and steel indenters have shown that the introduction of both 12 wt% [60] and 21 wt% [61] Hf into the coating based on the ZrN system can significantly increase its wear resistance. At the same time, when using the Al_2O_3 indenter, noticeable oxidation was observed, and the steel indenter mainly caused the mechanical destruction of the coating. The use of the (Zr,Hf)N coating also reduces the wear of both indenters—Al_2O_3 and steel [60]. A comparison of the wear resistance of a tool with Zr/Hf nitride and DLC coatings showed that the nitride coating formed stable oxide layers that slowed down diffusion wear [62]. Furthermore, glassy amorphous oxide layers were formed on the DLC coating. While the ZrN coating provides a lower COF when in contact with the Al_2O_3 indenter, it does not provide better wear resistance. Moreover, while the COF of the ZrN coating paired with the AISI 52100 indenter is almost identical to that of the uncoated sample, the wear resistance of the ZrN-coated sample in this pair is significantly higher compared to the uncoated one. Notably, the COF is Important but not the only factor determining the overall wear resistance of the coating. In both cases, the Indenter mass loss is minimal when in contact with the DLC-coated sample (Figure 7e,f).

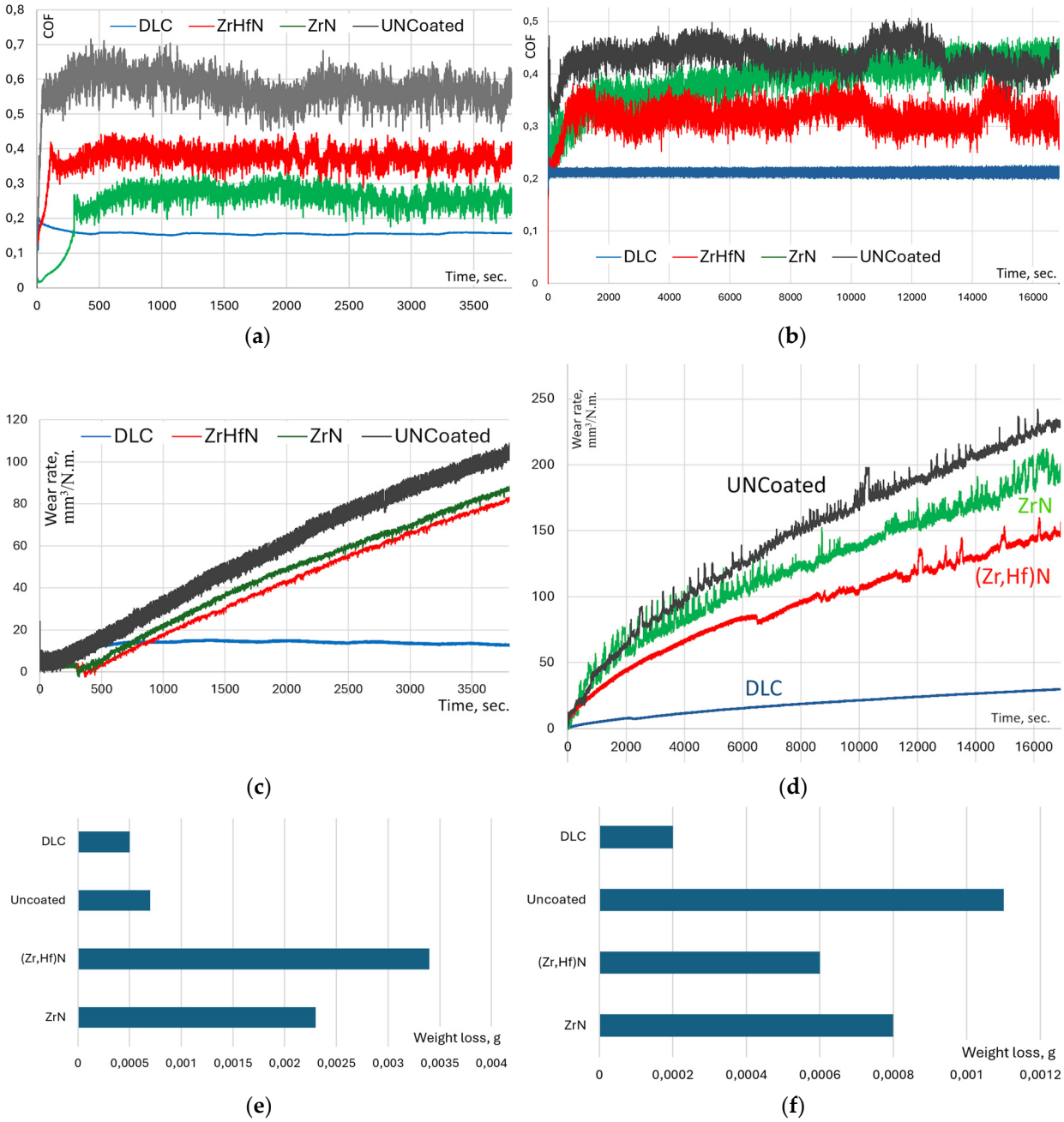

Figure 7. Tribological properties (coefficient of friction [COF]) and wear resistance in pin-on-disk tests: (**a**) COF in contact with Al_2O_3 indenter, (**b**) COF in contact with AISI 52100 indenter, (**c**) wear dynamics in contact with Al_2O_3 indenter, (**d**) wear dynamics in contact with AISI 52100 indenter, (**e**) mass loss of Al_2O_3 indenter, and (**f**) mass loss of AISI 52100 indenter.

Notably, there is a significant difference in the resistance to destruction of the DLC coating in the scratch and pin-on-disk tests. In the first case, the coating is actively destroyed by a brittle fracture mechanism, and in the second, an extremely low intensity of destruction is observed. Furthermore, there is a significant difference in the test conditions. If in the scratch test, the impact is exerted by an extremely sharp diamond indenter (diameter of 100 μm at the tip), then in the pin-on-disk test, the indenter diameter is 6 mm (6000 μm), and its hardness is noticeably lower (even in the case of Al_2O_3). Thus, as a hard and brittle material, DLC shows good resistance to loads that do not exceed specific values. Exceeding these specific load values can initiate active cracking and, accordingly, the destruction of this material.

3.3. Corrosion Resistance in Physiological Solution (0.9% NaCl)

The potentiodynamic polarization curves of the investigated (Zr,Hf)N, ZrN, and DLC coatings on the surface of the Ti-6Al-4V alloy in physiological solution (0.9% NaCl) are shown in Figure 8. Previous studies have indicated that ZrN and DLC coatings provide high corrosion resistance in Ringer's solution and 0.9% NaCl [63,64]. Furthermore, a comparison of the anticorrosive properties of ZrN and DLC coatings deposited on a medical TiNi alloy substrate showed that the ZrN coating provides better protection against corrosion in physiological solution [65]. In the obtained graph, on the anodic branch of the polarization curve of the DLC coating after the active dissolution region of +0.25 to +0.55 V, a local minimum of the anodic current density is observed at +0.65 V. This behavior can be explained by the formation of an oxide layer (oxidized DLC, see Figure 9) on the surface of the DLC coating and the subsequent self-passivation of the titanium base, as observed in the corrosion study of DLC-coated Ti-6Al-4V samples.

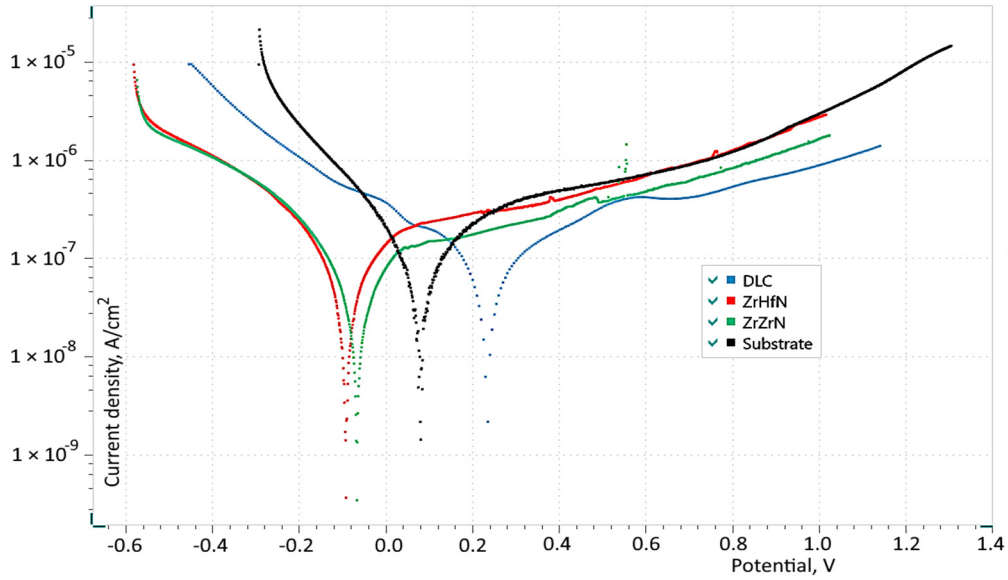

Figure 8. Superposition of potentiodynamic curves of the studied (Zr,Hf)N, ZrN, and DLC coatings on the surface of the Ti-6Al-4V alloy in 0.9% NaCl at 40 °C (Vp = 10 mV/s).

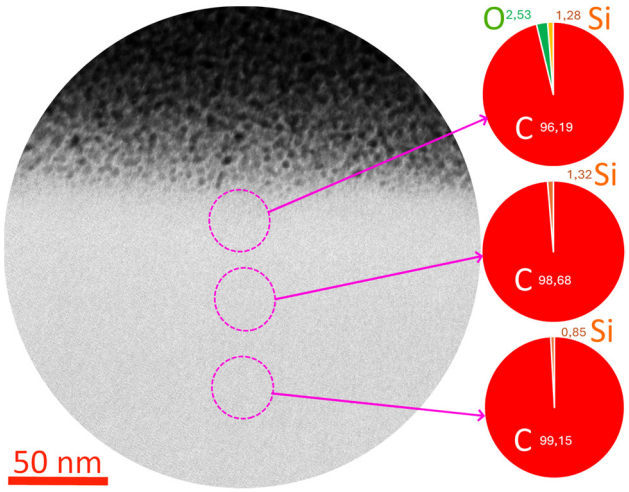

Figure 9. Oxidation processes in the DLC coating surface after exposure to 0.9% NaCl at 40 °C (Vp = 10 mV/s; TEM).

At the same time, the dissolution of the ZrN and (Zr,Hf)N nitride coatings in 0.9% NaCl at 40 °C occurs with the formation of the oxynitride and oxide of zirconium and

hafnium on the surface, respectively [40,46]. The electrochemical behavior of the nitride coatings differs significantly from that of DLC: the onset potentials of the corrosion process for the nitride coatings lie in the range of −0.091 to −0.066 V, which is significantly lower than the corrosion potential of the DLC coating, that is, +0.235 V (Table 1). The passive region for the nitride coatings is observed in the potential range of 0.00 to +0.15 V. Even though the corrosion potential shifts to the negative region, the corrosion current density of the nitride coatings is lower than that of the DLC coating: 30.8 and 37.0 nA/cm^2 for ZrN and (Zr,Hf)N, respectively, and 43.6 nA/cm^2 for DLC. These results indicate the higher corrosion resistance of the nitride coatings in a solution simulating blood plasma (0.9% NaCl); this occurs due to the dissolution of ZrN and HfN, with the formation of nonstoichiometric zirconium and/or hafnium oxychloride on the surface of the Ti-6Al-4V alloy [40,46] in chloride solutions.

Table 1. Calculated results of the corrosion process in the Nova 2.0 program by determining the polarization resistance in the corrosion potential region in 0.9% NaCl at 40 °C.

Coating	E_{corr}, V	Polarization Resistance Method		
		i_{corr}, nA/cm^2	II, μm/year	Ro, MΩ
ZrN	−0.066	30.8	0.272	0.846
(Zr,Hf)N	−0.091	37.0	0.326	0.704
DLC	+0.235	43.6	0.385	0.598
Uncoated	+0.081	63.5	0.560	0.410

One should note the 0.025 V shift in the corrosion potential for hafnium-doped zirconium nitride toward a more electronegative region compared to pure zirconium nitride, which indicates an increase in the corrosion processes in the former. The corrosion currents of the (Zr,Hf)N-coated samples do not exceed 37.01 nA/cm^2, which is 20% higher than the corrosion currents of the ZrN-coated samples. At the same time, the deposition of (Zr,Hf)N, ZrN, and DLC coatings on the surface of the Ti-6Al-4V alloy inhibits the dissolution currents by 30–40% and increases the polarization resistance to the corrosion process 1.5–2.0-fold compared to uncoated Ti-6Al-4V in 0.9% NaCl at 40 °C (see Table 1).

Thus, the deposition of (Zr,Hf)N, ZrN, and DLC coatings on the surface of the Ti-6Al-4V alloy samples slows down the corrosion dissolution of the base by 30–40% compared to the uncoated alloy. This phenomenon is caused by the formation of nonstoichiometric zirconium and/or hafnium oxychloride for the nitride coatings, and in the case of the DLC coatings, by the generation of a layer of oxidized DLC at +0.65 V and the subsequent self-passivation of the titanium base.

4. Conclusions

The properties of ZrN, (Zr,Hf)N, and DLC coatings deposited on a Ti-6Al-4V alloy substrate were compared. In the DLC coating deposition, preliminary etching with chromium ions was carried out, ensuring the formation of a diffusion surface layer saturated with chromium in the substrate. Thereafter, a Si-DLC layer followed by a pure DLC layer was deposited.

The following conclusions can be drawn from the analysis of the experimental data:

- The surface of the DLC coating contains microchips up to 100 μm in length, while such chips are not observed in the nitride coatings.
- During the scratch test, the DLC coating begins to break down even under small (from 6 N) loads via the spallation failure mechanism, while under large loads, the peeling off of large fragments of the coating can be observed. The breakage of the ZrN and (Zr,Hf)N nitride coatings occurs via a more plastic mechanism, and no noticeable peeling of the coatings is observed.

- During the pin-on-disk test in contact with the Al_2O_3 and AISI 52100 indenters, the DLC-coated sample demonstrates a much lower coefficient of friction and significantly better wear resistance compared to the nitride-coated samples.
- The deposition of ion-plasma coatings of (Zr,Hf)N, ZrN, and DLC on the surface of the Ti-6Al-4V alloy samples slows down the corrosive dissolution of the base by 30–40% compared to the uncoated sample. The corrosion currents observed in the (Zr,Hf)N-coated specimens do not surpass 37.01 nA/cm^2, representing an increase of 20% in comparison to the corrosion currents measured for the ZrN-coated specimens. Concurrently, applying (Zr,Hf)N, ZrN, and DLC coatings onto the surface of the Ti-6Al-4V alloy results in a significant reduction in the dissolution currents (by 30–40%) and an enhancement of the polarization resistance to corrosion (by a factor of 1.5–2.0) in relation to the uncoated Ti-6Al-4V in 0.9% NaCl at 40 °C.

Thus, the DLC coating of the described structure simultaneously provides effective wear and corrosion resistance in an environment simulating blood plasma (0.9% NaCl at 40 °C). That is, this coating can be effectively used in the generation of medical products (in particular, implants) from titanium alloys, including those functioning in the environment of the human body and subject to mechanical wear (e.g., knee joint endoprostheses).

Author Contributions: Conceptualization, A.M., A.V. and S.F.; methodology, S.F., Y.B., F.M., A.S., V.Z., V.C., Y.B. and C.S.; validation, F.M., A.S., Y.B. and C.S.; investigation, F.M., Y.B., A.S., V.Z., V.C., Y.B. and K.M.; resources, A.M.; data curation, A.M., V.Z. and V.C.; writing—original draft preparation, A.V.; writing—review and editing, A.V. and C.S.; supervision, A.M. and V.Z.; project administration, A.V. and C.S.; funding acquisition, A.M. All authors have read and agreed to the published version of the manuscript.

Funding: The research was financially supported by the Ministry of Science and Higher Education of the Russian Federation (project No. FSFS-2021-0006).

Data Availability Statement: The original contributions presented in the study are included in the article, further inquiries can be directed to the corresponding authors.

Conflicts of Interest: The authors declare no conflicts of interest.

References

1. Kong, W.; Yu, Z.; Hu, J. Electrochemical performance and corrosion mechanism of Cr–DLC coating on nitrided Ti6Al4V alloy by magnetron sputtering. *Diam. Relat. Mater.* **2021**, *116*, 108398.
2. Kumar, A.; Singh, G. Surface modification of Ti6Al4V alloy via advanced coatings: Mechanical, tribological, corrosion, wetting, and biocompatibility studies. *J. Alloys Compd.* **2024**, *989*, 174418. [CrossRef]
3. Kashyap, V.; Ramkumar, P. DLC coating over pre-oxidized and textured Ti6Al4V for superior adhesion and tribo-performance of hip implant. *Surf. Coat. Technol.* **2022**, *440*, 128492. [CrossRef]
4. Österle, W.; Klaffke, D.; Griepentrog, M.; Gross, U.; Kranz, I.; Knabe, C. Potential of wear resistant coatings on Ti–6Al–4V for artificial hip joint bearing surfaces. *Wear* **2008**, *264*, 505–517. [CrossRef]
5. Alakoski, E.; Tiainen, V.-M.; Soininen, A.; Konttinen, Y.T. Load-bearing biomedical applications of diamond-like carbon coatings-current status. *Open Orthop. J.* **2008**, *2*, 43–50. [CrossRef] [PubMed]
6. Al Jabbari, Y.S.; Fehrman, J.; Barnes, A.C.; Zapf, A.M.; Zinelis, S.; Berzins, D.W. Titanium nitride and nitrogen ion implanted coated dental materials. *Coatings* **2012**, *2*, 160–178. [CrossRef]
7. Affatato, S.; Frigo, M.; Toni, A. An in vitro investigation of diamond like carbon as a femoral head coating. *J. Biomed. Mater. Res.* **2000**, *53*, 221–226. [CrossRef]
8. Fisher, J.; Hu, X.Q.; Stewart, T.D.; Williams, S.; Tipper, J.L.; Ingham, E.; Stone, M.H.; Davies, C.; Hatto, P.; Bolton, J.; et al. Wear of surface engineered metal-on-metal hip prostheses. *J. Mater. Sci. Mater. Med.* **2004**, *15*, 225–235. [CrossRef] [PubMed]
9. Taeger, T.; Podleska, L.E.; Schmidt, B.; Ziegler, M.; Nast-Kolb, D. Comparison of diamond like carbon and alumina oxide articulating with polyethylene in total hip arthroplasty. *Materialwiss. Werkstofftech.* **2003**, *34*, 1094–1100. [CrossRef]
10. Xu, T.; Pruitt, L. Diamond Like Carbon coatings for orthopaedic applications: An evaluation of tribological performance. *J. Mater. Sci. Mater. Med.* **1999**, *10*, 83–90. [CrossRef]
11. Shiri, S.; Ashtijoo, P.; Odeshi, A.; Yang, Q. Evaluation of Stoney equation for determining the internal stress of DLC thin films using an optical profiler. *Surf. Coat. Technol.* **2016**, *308*, 98–100. [CrossRef]
12. Wang, P.; Wang, X.; Xu, T.; Liu, W.; Zhang, J. Comparing internal stress in diamond-like carbon films with different structure. *Thin Solid Films* **2007**, *515*, 6899–6903. [CrossRef]

13. Love, C.A.; Cook, R.B.; Harvey, T.; Dearnley, P.; Wood, R. Diamond like carbon coatings for potential application in biological implants—A review. *Tribol. Int.* **2013**, *63*, 141–150. [CrossRef]
14. Bonu, V.; Srinivas, G.; Praveen Kumar, V.; Joseph, A.; Narayana, C.; Barshilia, H.C. Temperature dependent erosion and Raman analyses of arc-deposited H free thick DLC coating on Cr/CrN coated plasma nitrided steel. *Surf. Coat. Technol.* **2021**, *436*, 128308. [CrossRef]
15. Liu, X.; Zhang, W.; Sun, G. The influence of textured interface on DLC films prepared by vacuum arc. *Surf. Coat. Technol.* **2019**, *365*, 143–151. [CrossRef]
16. Wei, C.; Yen, J.Y. Effect of film thickness and interlayer on the adhesion strength of diamond like carbon films on different substrates. *Diam. Relat. Mater.* **2007**, *16*, 1325–1330. [CrossRef]
17. Walkowicz, J.; Bujak, J.; Zavaleyev, V. The effect of unintentional oxygen incorporation into Cr-CrN-DLC coatings deposited by MePIIID method using filtered cathodic vacuum arc carbon and metal plasma. *Probl. At. Sci. Technol.* **2010**, *6*, 179–181.
18. Bujak, J.; Michalczewski, R. Characterization and properties of low-friction, multilayered Cr-doped diamond-like carbon coatings prepared by pulse biased filtered cathodic arc deposition. *Proc. Inst. Mech. Eng. B J. Eng. Manuf.* **2011**, *225*, 875–882. [CrossRef]
19. Hao, T.; Du, J.; Su, G.; Zhang, P.; Sun, Y.; Zhang, J. Mechanical and cutting performance of cemented carbide tools with Cr/x/DLC composite coatings. *Int. J. Adv. Manuf. Technol.* **2020**, *106*, 5241–5254. [CrossRef]
20. Al-Asadi, M.M.; Al-Tameemi, H.A. A review of tribological properties and deposition methods for selected hard protective coatings. *Tribol. Int.* **2022**, *176*, 107919. [CrossRef]
21. Crombez, R.; McMinis, J.; Veerasamy, V.S.; Shen, W. Experimental study of mechanical properties and scratch resistance of ultra-thin diamond-like-carbon (DLC) coatings deposited on glass. *Tribol. Int.* **2011**, *44*, 55–62. [CrossRef]
22. Khodayari, A.; Elmkhah, H.; Alizadeh, M.; Maghsoudipour, A. Modified diamond-like carbon (Cr-DLC) coating applied by PACVD-CAPVD hybrid method: Characterization and evaluation of tribological and corrosion behavior. *Diam. Relat. Mater.* **2023**, *136*, 109968. [CrossRef]
23. Danelon, M.R.; de Almeida, L.S.; Manfrinato, M.D.; Rossino, L.S. Study of the influence of a gradient gas flow as an alternative to improve the adhesion of Diamond-Like Carbon film in the wear and corrosion resistance on the nitrided AISI 4340 steel. *Surf. Interfaces* **2023**, *36*, 102352. [CrossRef]
24. Feng, X.; Hu, H.; Gui, B.; Guo, F.; Wang, K.; Zheng, Y.; Zhou, H. Corrosion behavior of W-DLC and DLC films deposited on plasma nitrided CF170 steel in H_2SO_4 solution. *Vacuum* **2022**, *204*, 111385. [CrossRef]
25. Zhang, L.; Shang, L.; Gou, C.; Zhang, G. Tribological and corrosive behavior under HCl corrosive environment of diamond-like carbon films with doped H, Cr and WC. *Surf. Coat. Technol.* **2024**, *482*, 130685. [CrossRef]
26. Marciano, F.R.; Bonetti, L.F.; Santos, L.V.; Da-Silva, N.S.; Corat, E.J.; Trava Airoldi, V.J. Antibacterial activity of DLC and Ag–DLC films produced by PECVD technique. *Diam. Relat. Mater.* **2009**, *18*, 1010–1014. [CrossRef]
27. Sovak, G.; Weiss, A.; Gotman, I. Osseointegration of Ti6Al4V alloy implants coated with titanium nitride by a new method. *J. Bone Jt. Surg. Br. Vol.* **2000**, *82*, 290–296. [CrossRef]
28. Huang, W.; Zalnezhad, E.; Musharavati, F.; Jahanshahi, P. Investigation of the tribological and biomechanical properties of CrAlTiN and CrN/NbN coatings on SST 304. *Ceram. Int.* **2017**, *43*, 7992–8003. [CrossRef]
29. Ramoul, C.; Beliardouh, N.E.; Bahi, R.; Nouveau, C.; Djahoudi, A.; Walock, M.J. Surface performances of PVD ZrN coatings in biological environments. *Tribol.-Mater. Surf. Interfaces* **2019**, *13*, 12–19. [CrossRef]
30. Sotova, C.; Yanushevich, O.; Krikheli, N.; Kramar, O.; Vereschaka, A.; Shehtman, S.; Milovich, F.; Zhylinski, V.; Seleznev, A.; Peretyagin, P. Influence of Nitride Coatings on Corrosion Resistance and the Biocompatibility of Titanium Alloy Products. *Metals* **2024**, *14*, 1200. [CrossRef]
31. Noori, M.; Atapour, M.; Ashrafizadeh, F.; Elmkhah, H.; di Confiengo, G.G.; Ferraris, S.; Perero, S.; Cardu, M.; Spriano, S. Nanostructured multilayer CAE-PVD coatings based on transition metal nitrides on Ti6Al4V alloy for biomedical applications. *Ceram. Int.* **2023**, *49*, 23367–23382. [CrossRef]
32. Cotrut, C.-M.; Braic, V.; Balaceanu, M.; Titorencu, I.; Braic, M.; Parau, A.C. Corrosion resistance, mechanical properties and biocompatibility of Hf-containing ZrCN coatings. *Thin Solid Films* **2013**, *538*, 48–55. [CrossRef]
33. Cui, W.; Cheng, J.; Liu, Z. Bio-tribocorrosion behavior of a nanocrystalline TiZrN coating on biomedical titanium alloy. *Surf. Coat. Technol.* **2019**, *369*, 79–86. [CrossRef]
34. Cai, F.; Zhou, Q.; Chen, J.; Zhang, S. Effect of inserting the Zr layers on the tribo-corrosion behavior of Zr/ZrN multilayer coatings on titanium alloys. *Corros. Sci.* **2023**, *213*, 111002. [CrossRef]
35. Atar, E.; Cimenolu, H.; Kayali, E.S. Hardness characterisation of thin Zr(Hf,N) coatings. *Surf. Coat. Technol.* **2003**, *162*, 167–173. [CrossRef]
36. Atar, E.; Kayali, E.S.; Cimenoglu, H. The effect of oxidation on the structure and hardness of (Zr,Hf)N coatings. *Defect Diffus. Forum* **2011**, *297–301*, 1395–1399. [CrossRef]
37. Vereschaka, A.; Milovich, F.; Andreev, N.; Seleznev, A.; Alexandrov, I.; Mikhailov, A.; Tatarkanov, A. Comparison of properties of ZrHf-(Zr,Hf)N-(Zr,Hf,Cr,Mo,Al)N and Ti-TiN-(Ti,Cr,Al)N nanostructured multilayer coatings and cutting properties of tools with these coatings during turning of nickel alloy. *J. Manuf. Process.* **2023**, *88*, 184–201. [CrossRef]
38. Vereschaka, A.; Milovich, F.; Andreev, N.; Migranov, M.; Alexandrov, I.; Muranov, A.; Mikhailov, M.; Tatarkanov, A. Specific Application Features of Ti-TiN-(Ti,Cr,Al)N, Zr-ZrN-(Zr,Mo,Al)N, and ZrHf-(Zr,Hf)N-(Zr,Hf,Cr,Mo,Al)N Multilayered Nanocomposite Coatings in End Milling of the Inconel 718 Nickel-Chromium Alloy. *J. Compos. Sci.* **2022**, *6*, 382. [CrossRef]

39. Wu, Z.T.; Qi, Z.B.; Zhang, D.F.; Wang, Z.C. Microstructure, mechanical properties and oxidation resistance of (Zr,Hf)N_x coatings by magnetron co-sputtering. *Surf. Coat. Technol.* **2015**, *276*, 219–227. [CrossRef]
40. Tao, H.; Zhylinski, V.; Vereschaka, A.; Keshin, A.; Huo, Y.; Milovich, F.; Sotova, C.; Seleznev, A. Influence of niobium and hafnium doping on the wear and corrosion resistance of coatings based on ZrN. *J. Mater. Res. Technol.* **2023**, *27*, 6386–6399.
41. Aslan, N.; Aksakal, B.; Cihangir, S.; Cetin, F.; Yilmazer, Y. ZrN and ta-C coatings on titanium for biomedical applications: Improved adhesion, corrosion, antibacterial activity, and cytotoxicity properties. *J. Mater. Res.* **2023**, *38*, 3923–3936. [CrossRef]
42. Hajduga, M.B.; Bobinski, R. TiN, ZrN and DLC nanocoatings—A comparison of the effects on animals, in-vivo study. *Mater. Sci. Eng. C* **2019**, *104*, 109949. [CrossRef] [PubMed]
43. Cui, M.; Pu, J.; Zhang, G.; Wang, L.; Xue, Q. The corrosion behaviors of multilayer diamond-like carbon coatings: Influence of deposition periods and corrosive medium. *RSC Adv.* **2016**, *6*, 28570–28578. [CrossRef]
44. Zhang, T.F.; Deng, Q.Y.; Liu, B.; Wu, B.J.; Jing, F.; Leng, Y.; Huang, N. Wear and corrosion properties of diamond like carbon (DLC) coating on stainless steel, CoCrMo and Ti6Al4V substrates. *Surf. Coat. Technol.* **2015**, *273*, 12–19. [CrossRef]
45. Han, B.B.; Ju, D.Y.; Chai, M.R.; Zhao, H.J.; Sato, S. Corrosion Resistance of DLC Film-Coated SUS316L Steel Prepared by Ion Beam Enhanced Deposition. *Adv. Mater. Sci. Eng.* **2019**, *2019*, 480618. [CrossRef]
46. Tao, H.; Zhylinski, V.; Vereschaka, A.; Chayeuski, V.; Yuanming, H.; Milovich, F.; Sotova, C.; Seleznev, A.; Salychits, O. Comparison of the Mechanical Properties and Corrosion Resistance of the Cr-CrN, Ti-TiN, Zr-ZrN, and Mo-MoN Coatings. *Coatings* **2023**, *13*, 750. [CrossRef]
47. Grigoriev, S.N.; Volosova, M.A.; Fedorov, S.V.; Migranov, M.S.; Mosyanov, M.; Gusev, A.; Okunkova, A.A. The Effectiveness of Diamond-like Carbon a-C:H:Si Coatings in Increasing the Cutting Capability of Radius End Mills When Machining Heat-Resistant Nickel Alloys. *Coatings* **2022**, *12*, 206. [CrossRef]
48. Grigoriev, S.; Vereschaka, A.; Milovich, F.; Sitnikov, N.; Bublikov, J.; Seleznev, A.; Sotova, C. Crack formation and oxidation wear in (Cr,Y,Al)N and (Mo,Y,Al)N nanolayer coatings with high content of yttrium. *Wear* **2023**, *528–529*, 204989. [CrossRef]
49. Grigoriev, S.; Vereschaka, A.; Zelenkov, V.; Sitnikov, N.; Bublikov, J.; Milovich, F.; Andreev, N.; Sotova, C. Investigation of the influence of the features of the deposition process on the structural features of microparticles in PVD coatings. *Vacuum* **2022**, *202*, 111144. [CrossRef]
50. Grigoriev, S.; Vereschaka, A.; Zelenkov, V.; Sitnikov, N.; Bublikov, J.; Milovich, F.; Andreev, N.; Mustafaev, E. Specific features of the structure and properties of arc-PVD coatings depending on the spatial arrangement of the sample in the chamber. *Vacuum* **2022**, *200*, 111047. [CrossRef]
51. *ASTM C1624-22*; Standard Test Method for Adhesion Strength and Mechanical Failure Modes of Ceramic Coatings by Quantitative Single Point Scratch Testing. 2022. Available online: https://www.astm.org/c1624-22.html (accessed on 22 June 2024).
52. *ASTM G99-23*; Standard Test Method for Wear and Friction Testing with a Pin-on-Disk or Ball-on-Disk Apparatus. 2023. Available online: https://cdn.standards.iteh.ai/samples/116624/e0d864e0711e4750be5b58945c0bf1c4/ASTM-G99-23.pdf (accessed on 22 June 2024).
53. Meija, J.; Coplen, T.; Berglund, M.; Brand, W.; De Bièvre, P.; Gröning, M.; Holden, N.; Irrgeher, J.; Loss, R.; Walczyk, T.; et al. Atomic weights of the elements 2013 (IUPAC Technical Report). *Pure Appl. Chem.* **2016**, *88*, 265–291. [CrossRef]
54. Burnett, P.J.; Rickerby, D.S. The Relationship Between Hardness and Scratch Adhesion. *Thin Solid Films* **1987**, *154*, 403–416. [CrossRef]
55. Nyemchenko, U.S.; Beresnev, V.M.; Gorban, V.F.; Novikov, V.J.; Yaremenko, O.V. Comparing the tribological properties of the coatings (Ti-Hf-Zr-V-Nb-Ta)N and (Ti-Hf-Zr-V-Nb-Ta)N + DLC. *J. Nano Electron. Phys.* **2015**, *7*, 03041.
56. Ostrovskaya, Y.L.; Strel'nitskij, V.E.; Kuleba, V.I.; Gamulya, G.D. Friction and wear behaviour of hard and superhard coatings at cryogenic temperatures. *Tribol. Int.* **2001**, *34*, 255–263. [CrossRef]
57. Yin, Z.; Liang, G.; Bi, J. High strength and hardness BNNSs/Al_2O_3 composite ceramics prepared by hot-press sintering of in-situ composite BNNSs/Al_2O_3 powder. *Ceram. Int.* **2023**, *49*, 31794–31801. [CrossRef]
58. Zhong, Y.; Xiang, W.; He, L.; Li, J.; Hao, J.; Tian, Z.; Wang, X. Directionally solidified Al_2O_3/$(Y_{0.2}Er_{0.2}Yb_{0.2}Ho_{0.2}Lu_{0.2})_3Al_5O_{12}$ eutectic high-entropy oxide ceramics with well-oriented structure, high hardness, and low thermal conductivity. *J. Eur. Ceram. Soc.* **2021**, *41*, 7119–7129. [CrossRef]
59. *AISI 52100*; Alloy Steel (UNS G52986) by AZoNetwork, Manchester, United Kingdom. 2024. Available online: https://www.azom.com/article.aspx?ArticleID=6704 (accessed on 22 June 2024).
60. Atar, E.; Kayali, E.S.; Cimenoglu, H. Sliding wear behaviour of ZrN and (Zr, 12 wt% Hf)N coatings. *Tribol. Int.* **2006**, *39*, 297–302. [CrossRef]
61. Atar, E.; Kayali, E.S.; Cimenoglu, H. Reciprocating wear behaviour of (Zr, Hf)N coatings. *Wear* **2004**, *257*, 633–639. [CrossRef]
62. Bushlya, V.; Johansson, D.; Lenrick, F.; Ståhl, J.-E.; Schultheiss, F. Wear mechanisms of uncoated and coated cemented carbide tools in machining lead-free silicon brass. *Wear* **2017**, *376–377*, 143–151. [CrossRef]
63. Hajduga, M.B.; Was-Solipiwo, J.; Wegrzynkiewicz, S.; Hajduga, M.A. Corrosion and bacterial resistance of ZrN, DLC comp A-C:H and multicomp tin/tialn coatings used in medical. In Proceedings of the METAL 2015—24th International Conference on Metallurgy and Materials, Brno, Czech Republic, 3–5 June 2015; pp. 935–940.

64. Asadian, K.; Samiee, M.; Mafi, M. Wear Mechanism and Electrochemical Properties of Different Interlayers on DLC Film Deposited by PECVD Technique. *J. Bio-Tribo-Corros.* **2024**, *10*, 30. [CrossRef]
65. Urban, V.I.; Rubanik, V.V.; Rubanik, V.V., Jr.; Bagrets, D.A.; Dorodeiko, V.G.; Vieira, D.E.L.; Salak, A.N. Corrosion Properties of TiNi Medical Alloy with Bioinert Coatings. *Prot. Met. Phys. Chem. Surf.* **2023**, *59*, 717–723. [CrossRef]